A Multiband 4th-Order RF Transmitter Featuring an N-Path-Filter Modulator with a Switched g_m-C Network Achieving 230MHz Signal Bandwidth

Gengzhen Qi[1*], Yunchu Li[1], Shaolin Liao[2] and Pui-In Mak[3]

[1]School of Microelectronics Science and Technology, Sun Yat-sen University, Zhuhai, China
[2]School of Electronics and Information Technology, Sun Yat-sen University, Guangzhou, China
[3]State-Key Laboratory of Analog and Mixed-Signal VLSI/Institute of Microelectronics, University of Macau, Macao, China
[*] Email: qigzh@mail.sysu.edu.cn

***Abstract*—A multiband RF transmitter featuring a switched transconductance (g_m)-C network embedded into its N-path-filter modulator for bandwidth (BW) extension is described. It exhibits a 4th-order high-Q bandpass response by applying the "subtraction" method of two N-path networks that have poly-phase g_m cells for shifting the baseband (BB) admittance. After subtraction at the two outputs, the transmitter shows a wide passband BW (230MHz), while effectively suppressing the out-of-band (OB) noise and replicas. Unlike the typical transmitter with high-order BB low-pass filters that can suppress only the noise of the DACs, our transmitter can also attenuate the noise due to the BB circuitry, mixer and power amplifier (PA) driver. To enhance the transmitter efficiency and preserve the linearity, the PA driver exploits a Class-A/B transconductor parallelized with a linearizer biased in the triode region. The transmitter fabricated in 65nm CMOS shows ≤-156.3dBc/Hz OB noise and <-41.6dBc ACLR$_1$ for 1.4-to-2.7GHz RF range. The power consumption is 61.9mW at a 2.9dBm output power and the active area is 0.29mm^2.**

Keywords*—BW-extended, high-Q bandpass response, multiband, N-path filter-modulator, radio frequency (RF), switched g_m-C, subtraction, transmitter.

I. Introduction

With the evolution of the 5G New Radio (NR) and beyond, the implementation of the RF transmitters continue to face the challenges of wider signal bandwidth (BW), higher linearity and lower output noise. For frequency-division duplex (FDD) mode, 3GPP defines a maximum 100MHz signal BW, meanwhile with <2xBW frequency space (Δf) between the transmitters and receivers. The small ratio of Δf/BW imposes a stringent output noise requirement to avoid desensitizing the near-band receivers, thus high-order filtering is needed for transmitters to attenuate the out-of-band (OB) noise and replicas of DACs. Besides, a high linearity (e.g., ACLR and EVM) is crucial to support high-quality data transmission. In [1], the current-mode transmitter introduces the high-order baseband (BB) filter and power-hungry power mixer, achieving -158dBc/Hz OB noise, while consuming >90mW and ~1mm^2 die area. In [2], the transmitter employs a resistive charge-domain DAC circuitry and passive mixers. The die area is only 0.22mm^2, but the output power is limited to -3.5dBm. Beyond that, the transmitter based on the N-path-filter modulator becomes a promising solution. In [3], the transmitter embeds a transformer-based N-path filter into the modulator and realizes a tunable bandpass response covering 2-to-3GHz RF range. The OB noise is attenuated to <-157dBc/Hz, but the signal BW is limited to 10MHz, which is due to the trade-off of the N-path filters between OB rejection and signal BW. To break such trade-off, in [4] the "subtraction" method showed a 4th-order bandpass filtering response by shifting the BB admittance with poly-phase g_m cells.

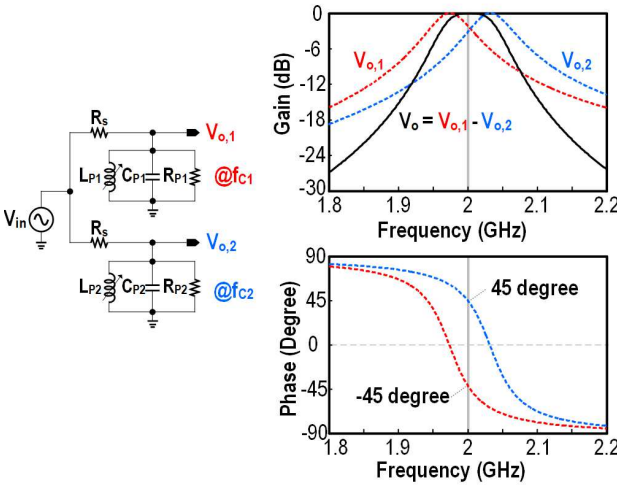

Fig. 1. "Subtracting" tunable 2nd-order RLC tanks achieves 4th-order bandpass filtering, where the in-band signals add up while the OB signals cancel each other.

Herein, we propose the "subtraction" method on our multiband wide-BW transmitter by embedding a switched g_m-C network into an N-path-filter modulator. After "subtraction" at the differential outputs of the power amplifier (PA) driver, the transmitter achieves both wide BW (230MHz) and high-Q bandpass filtering to attenuate the OB noise and replicas of DACs.

II. Concept of BW Extension

A 4th-order bandpass filter response can be obtained by subtracting two filters with the gain responses shifted up/down slightly [4]. In Fig. 1, when setting the two 2nd-order RLC tanks with an equal passband BW but with different center frequencies (i.e., f_{C1} and f_{C2}) by tuning inductors L_{P1} and L_{P2}, it manifests that the output of the RLC tanks ($V_{o,1}$ and $V_{o,2}$) present 45° offset from 0° for in-band signals, while almost in-phase for OB signals. Thus, under subtraction (i.e., $V_{o,1}$-$V_{o,2}$) we obtain the in-band signals while OB signals are cancelled. Such subtraction can be proposed to our transmitter by introducing two tunable 2nd-order RLC tanks at the following modulators (passive switches SW_L and SW_R).

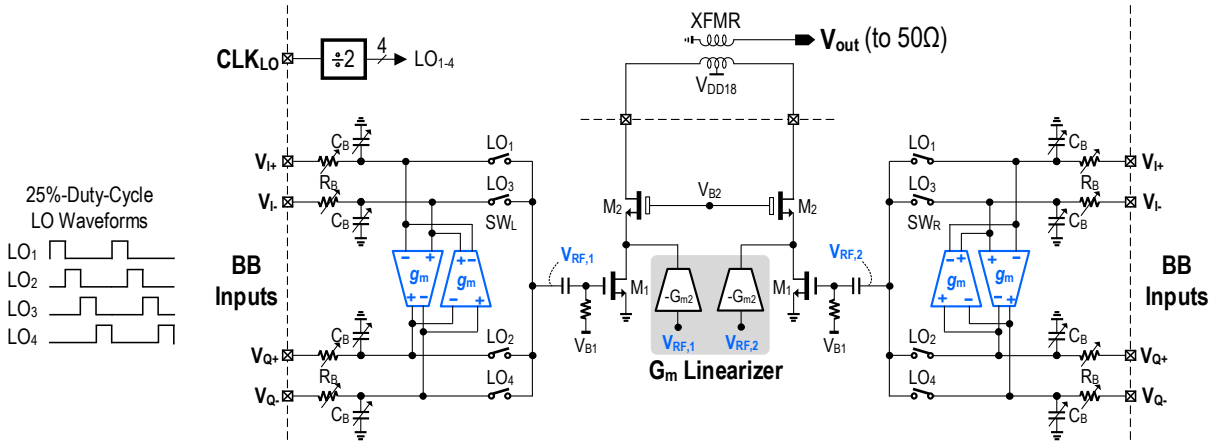

Fig. 2. Proposed BW-extended filter-modulator by "subtracting" two N-path SC modulators with switched g_m-C network to achieve 4th-order bandpass filtering. Multi-gate technique is applied on the PA driver to improve linearity.

After subtraction, i.e., $V_{RF,1}$-$V_{RF,2}$, we get a 4th-order BW-extended bandpass filter modulator. The tunable 2nd-order RLC tanks can be replaced by the N-path switched-capacitor filters operating at f_{C1} and f_{C2}, respectively.

III. Circuit Details

The schematic of our transmitter is depicted in Fig. 2, which comprises BB circuitry, modulator and PA driver. The 4-phase BB signals (i.e., I/Q and differential) are injected by tunable RC networks (R_B and C_B) and modulated (i.e., up-mixed) via SW_L and SW_R. Switches SW_L and SW_R in each path are driven by non-overlap 25%-duty-cycle LO waveforms (LO_{1-4}) and the center frequency is defined by f_{LO}.

A. BW-Extended N-Path-Filter Modulator

By introducing the switched g_m-C networks, our BW-extended N-path-filter modulator can be created in Fig. 2. The switched g_m-C networks shift the center frequency of N-path filters, in which 4-phase g_m cells are introduced to shift the BB admittance from $j\omega C_B$ to $j(\omega\pm\Delta\omega)C_B$. $\Delta\omega$ is equal to g_m/C_B. The shifted RF signals at $V_{RF,1}$ and $V_{RF,2}$ are then amplified by the PA drivers. After subtracting the signals at the output of PA drivers by using a balun, eventually we get the 4th-order bandpass filtering response. In simulation, the steep filter response at $V_{RF,1}$-$V_{RF,2}$ achieves 13.8dB OB rejection at 1xBW offset in Fig. 3, when the transconductance of BB g_m cell is 2.6mS, R_B=500Ω and C_B=5pF. The passband BW is 230MHz. When compared to the modulator without the switched g_m-C network, the OB rejection is improved 8.6dB. When tuning g_m from 1.6 to 3.1mS, the shifting frequency $\Delta\omega$ increases and extends signal BW from 135 to 280MHz, with ~6.6dB decrease for OB rejection at 1xBW offset. Here, $\Delta\omega$ is irrelative to R_B, but R_B plays an important role on adjusting the Q factor of the gain response. Besides, C_B allows balancing the performance of OB rejection and output noise. A small output noise can be obtained by enlarging C_B. When C_B is 5pF, the OB noise at $V_{RF,1}$ is simulated 0.82aV^2/Hz at 1xBW offset. The g_m cell employs a differential source-degenerated circuitry to improve the linearity. The center-frequency shifting in the gain response is due to the input parasitic capacitance of the PA driver. Note that output response of our transmitter suppresses the even-order harmonics of f_{LO}, since the signals are canceled after subtraction due to no frequency shifting happens.

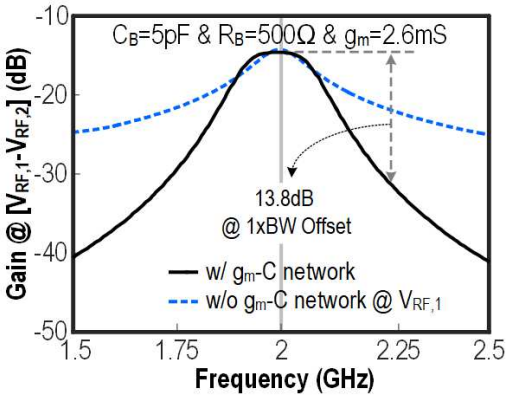

Fig. 3. Simulated gain response at $V_{RF,1}$–$V_{RF,2}$, showing that "Subtraction" method with switched g_m-C network improves OB rejection.

B. Linearized PA Driver

The primary source of nonlinearity in our transmitter stems from the PA driver, specifically due to the nonlinear voltage-to-current conversion in the input transistor M_1 in Fig. 2. The drain current i_{DS} of M_1 can be modeled as:

$$i_{DS} = I_{DC} + g_m \cdot v_{gs} + (g_m'/2!) \cdot v_{gs}^2 + (g_m''/3!) \cdot v_{gs}^3 + \cdots \quad (1)$$

Here, g_m' and g_m" denote the 1st- and 2nd-order derivatives of the transconductance with respect to the gate-source voltage (v_{gs}). The cubic term (v_{gs}^3) is particularly critical as it introduces 3rd-order distortion (e.g., CIM_3). To mitigate this nonlinearity, we adopt a multi-gate linearization technique. In Fig. 2, a g_m linearizer ($-G_{m2}$) is parallelized with the main g_m ($-G_{m1}$, transistor M_1) to neutralize its 3rd-order distortion. $-G_{m1}$ and $-G_{m2}$ are biased in the saturation and triode region, respectively. Besides, the PA driver operates in the Class-A/B mode to enhance the transmitter efficiency. $-G_{m1}$ and $-G_{m2}$ are NMOS devices and sized with 240µm/60 nm and 120µm/60nm, respectively. By incorporating the g_m linearizer, the out-of-band third-order intercept point (OB-IIP_3) of the PA driver is enhanced by 8.5dB relative to the non-linearized configuration and achieves 24dBm.

C. 25%-Duty-Cycle LO Generator

The 25%-duty-cycle LO generator is shown in Fig. 4, which comprises differential input buffer, div-by-2, AND

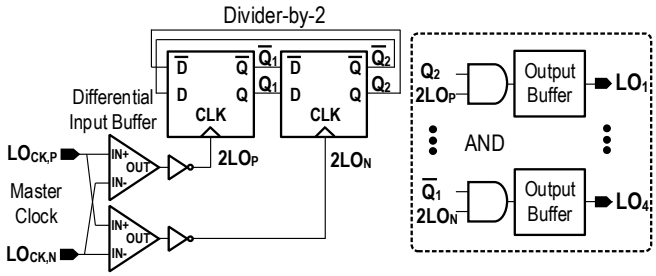

Fig. 4. 25%-duty-cycle LO generator.

logic and the output buffer. The differential master clocks $LO_{CK,P}$ and $LO_{CK,N}$ that operate at $2xf_{LO}$ are fed to the circuitry and amplified by the differential input buffer. After injecting to div-by-2, we obtain the 50%-duty-cycle LO waveforms Q_1, $\overline{Q_1}$, Q_2 and $\overline{Q_2}$. When applying AND logic (e.g., $2LO_P$ "AND" Q_2), the 25%-duty-cycle LO waveforms are generated. In order to drive the N-path switches, output buffer is employed to amplify the 25%-duty-cycle LO waveforms. Here, the output buffer can be tuned to adjust the pulse width of the LO waveforms by changing transistor size of PMOS and NMOS. The LO generator shows low-noise property, since the div-by-2 does not contribute noise due to the falling and rising edges are from $2LO_P$ and $2LO_N$. The differential input buffer improves the phase noise by ~6dB when compared to the single-ended inverter buffer. From simulations, the dynamic power is 5.5mW/GHz and the phase noise is -162.1dBc/Hz at 80MHz offset.

IV. Measurement Results

Fabricated in 65nm CMOS, our transmitter occupies 0.29mm^2 area, which is shown in Fig. 5. The power supply for the LO generator is 1.2V. An off-chip balun is employed to provide the power supply (1.8V) for the PA driver and also to obtain the output signal at V_{out} (Fig. 2) by subtracting the amplified signals of PA drivers. The high-Q bandpass gain responses are measured for different NR bands at 1.4 to 2.7GHz by tuning f_{LO}, which is shown in Fig. 6. When injecting 64 quadrature-amplitude modulation (QAM) single-carrier FDMA signal, the measured output spectrum is shown in Fig. 7, in which the output power is measured 2.9dBm at 2.535GHz with a 40MHz signal BW. The $ACLR_1$ and $ACLR_2$ are measured -41.6 and -50.3dBc, respectively, and the EVM is 2.3%. Note that the signal BW is limited by the signal generator in measurement. In Fig. 8, the output noise is ≤-156.3dBc/Hz at 1xBW offset for different NR bands, including both the thermal noise in signal path, g_m cells and the modulated phase-noise of LO generator. Enlarging C_B can further attenuate output noise. The measured CIM_3 and CIM_5 are <-53.8 and <-63.2dBc, respectively. The $ACLR_1$ ($ACLR_2$) is measured ≤-41.6dBc (≤-50.3dBc) for different NR bands, which is shown in Fig. 9. The power consumption is from 53.1mW (NR-n74) to 61.9mW (NR-n7 band), in which the power increase is due to the dynamic power of LO generator. Under power back-off, the power consumption reduces to 40.2mW for NR-n7 band. In addition, the measured $ACLR_{1,2}$ variation is <3dB when backing-off the output power.

The transmitter performance is summarized in Table I and compares it with the prior art [2, 3], [5-9]. Our transmitter features wide signal BW, sharp OB rejection and high

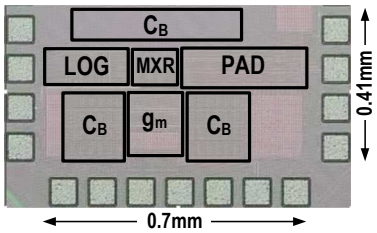

Fig. 5. Chip micrograph of the realized multiband RF transmitter in 65nm CMOS.

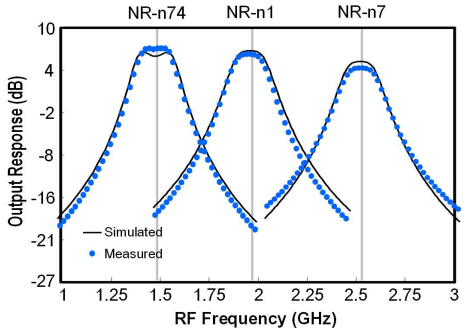

Fig. 6. Measured and simulated bandpass responses at different NR bands.

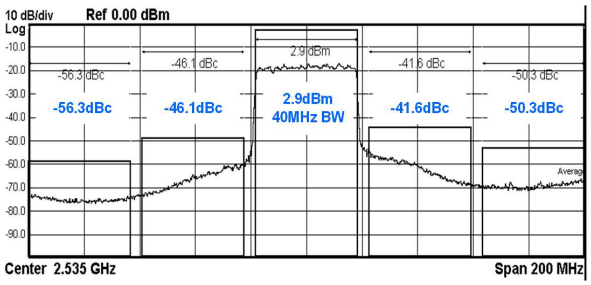

Fig. 7. Measured output spectrum for NR-n7 (2.535GHz) with a 40MHz BW.

transmitter efficiency. Compared to [5, 7, 8], our work has a 11.5x wider signal BW, a higher transmitter efficiency and also a smaller area. Although [2] reports a smaller OB noise than this work, it achieves 6.4dB lower output power and 11.5x narrower signal BW than our work. With similar OB noise as [3, 9], our work has a 23x wider signal BW. Compared to [6], our transmitter provides a 2.3x wider signal BW, a 1.6x higher transmitter efficiency and with comparable linearity.

V. Conclusions

A multiband BW-extended RF transmitter is presented by embedding a switched g_m-C network into an N-path-filter modulator to shift the BB admittance with poly-phase g_m cells in the BB. When applying the "subtraction" method at the output of the transmitter, we obtain a 4th-order response with a 230MHz passband BW and a high-Q bandpass response to attenuate OB noise and replicas. Our transmitter can suppress the noise due to BB circuitry, mixer and also the PA driver. The PA driver employs a Class-A/B transconductor parallelized with a linearizer biased in the triode region to to enhance the transmitter efficiency and also preserve the linearity. Fabricated in 65nm CMOS, it shows ≤156.3dBc/Hz OB noise and <-41.6dBc $ACLR_1$ for 1.4 to 2.7GHz RF range. It exhibits a 2.9dBm output power under 61.9mW power consumption. The active area is 0.29mm^2.

TABLE I. Comparison with State-of-the-Arts

	This Work	RFIC'24 [3]	ISSCC'20 [6]	JSSC'20 [7]	ISSCC'18 [5]	RFIC'18 [8]	ISSCC'16 [2]	JSSC'17 [9]
TX Techniques	N-Path SC MOD + g_m-C Network + PAD	N-Path SC-XFMR Filtering MOD + PAD	Harmonic-Rejection MXR + PAD	BW-Extended Filter-MOD + PAD	Tracking-Notch-Filter Mixer + PAD	Passive Mixer + Linearized PAD	Resistive QDAC + Passive Mixer	N-Path SC Gain Loop + PAD
RF Range (GHz)	1.4 to 2.7	2 to 3	2.3 to 5.0	1.4 to 2.7	1.4 to 2.7	2.3 to 3.6	0.9, 2.4	0.7 to 2
RF BW (MHz)	230	10	100	20	20	20	20	10
Output Power (dBm)	2.9	2.3	6.0	3.0	3.1	4	-3.5	-1
Power Cons. (mW)	61.9	33.6	210	70.5	113.2	159	24.8	38.4
TX Efficiency (%)	3.1	5.1	1.9	2.8	1.8	1.6	1.8	2.1
Output Noise (dBc/Hz) @ Δf (MHz)	-156.3 @ 1xBW	-157.6 @ 8xBW	-156 @ 1.2xBW #	-158 @ 6xBW	-157.8 @ 4xBW	-156 @ 5xBW	-158.9 @ 2.5xBW	-154.5 @ 8xBW
CIM_3 (dBc)	-53.8	-61	-71	-54	-59.6	-54.2	<-50	-52
$ACLR_1$ (dBc)	-41.6	-46	-45	-44.4	-44.7	-49	-47	-40.3
EVM (%)	2.3	2.2	1.9	1.9	N/R	1.8	<1.6	2.0
Active Area (mm^2)	0.22	0.21	0.195	0.31	1.04	0.85	0.22	0.038
Supply Voltage (V)	1.2, 1.8	1.2, 1.8	0.9, 1.8	1, 1.8	N/R	N/R	0.9, 1.1	1.1, 2.5
CMOS Tech. (nm)	65	65	12	28	14	40	28	65

N/R: Not reported #: Output noise measured at 0.5dBm output power

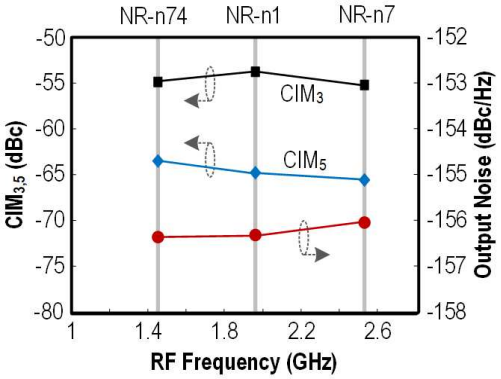

Fig. 8. Measured $CIM_{3,5}$ and output noise for different NR bands.

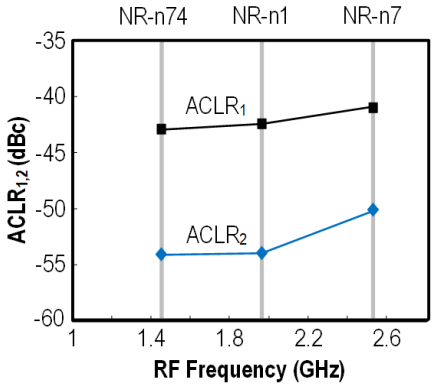

Fig. 9. Measured $ACLR_{1,2}$ for different NR bands.

ACKNOWLEDGMENT

This work is funded in part by the GuangDong Basic and Applied Basic Research Foundation under Grant 2025A1515011608; and in part by Guangdong Zhujiang Project under Grant 2021ZT09X070. It is also partially funded by the Guangdong-Hong Kong-Macao Joint Laboratories (GDSTC Project No. 2025B1212150003, FDCT File No. 001/2024/COP), and the Macau FDCT Fund (File No. 004/2023/SKL).

REFERENCES

[1] N. Codega, P. Rossi, A. Pirola, A. Liscidini and R. Castello, "A current-mode, low out-of-band noise LTE transmitter with a class-A/B power mixer," *IEEE J. of Solid-State Circuits*, vol. 49, pp. 1627-1638, Jul. 2014.

[2] P. Filho, M. Ingels, P. Wambacq and J. Craninckx, "A 0.22mm^2 CMOS resistive charge-based direct-launch digital transmitter with -159dBc/Hz out-of-band noise," in *ISSCC Dig. Tech. Papers*, pp. 250-252, Feb. 2016.

[3] G. Qi *et al.*, "A SAW-less 3f_{LO}-suppression RF transmitter with a transformer-based switched-capacitor modulator achieving -157.6dBc /Hz output noise and -61dBc CIM_3," in *Proc. IEEE RFIC Symp.*, pp. 259-262, Jun. 2024.

[4] M. Darvishi *et al.*, "Widely tunable 4th order switched G_m-C band-pass filter based on N-path filters," *IEEE J. of Solid-State Circuits*, vol. 47, no. 12, pp. 3105-3119, Dec. 2012.

[5] Q. Liu, D. Kwon, Q. Bui, *J. Choi, J. Lee, S. Baek, S. Heo and T. B. Cho,* "A 1.4-to-2.7GHz high-efficiency RF transmitter with an automatic 3FLO-suppression tracking-notch-filter mixer supporting HPUE in 14nm FinFET CMOS," in *ISSCC Dig. Tech. Papers*, pp. 172-174, Feb. 2018.

[6] M.-D. Tsai, C.-W. Tseng, K.-J. Tsai, S. Andrabi, P.-C. Huang, F. Beffa, Y. Chen and B. Tenbroek, "A 4G/5G cellular transmitter in 12nm FinFET with harmonic rejection," in *ISSCC Dig. Tech. Papers*, pp. 182-184, Feb. 2020.

[7] G. Qi, H. Shao, P.-I. Mak, J. Yin and R. P. Martins, "A multiband FDD SAW-less transmitter for 5G-NR featuring a BW-extended N-path filter-modulator, a switched-BB input and a wideband TIA-based PA driver," *IEEE J. of Solid-State* Circuits, vol. 55, no. 12, pp. 3387-3399, Dec. 2020.

[8] Y. Chen, A. Werquin, M. Hassan, C. Beghein, B. Tenbroek, J. Strange, C.-T. Chen, T.-H. Wu, Y.-H. Chen and C.-S. Chiu, "A Wideband Transmitter for LTE-A HPUE using CIM3 Cancellation," in *Proc. IEEE RFIC Symp.*, pp. 312-315, Jun. 2018.

[9] G. Qi, P.-I. Mak and R. P. Martins, "A 0.038mm^2 SAW-less multiband transceiver using an N-Path SC gain loop," *IEEE J. of Solid-State Circuits*, vol. 52, pp. 2055-2070, Aug. 2017.